J. Geophys. 43, 95 – 113, 1977

Journal of Geophysics

Three-Dimensional Seismic Ray Tracing

B. R. Julian [1] * and D. Gubbins [2]

[1] U.S. Geological Survey, Stop 968, Box 25046, Denver Federal Center, Denver, Co 80225, USA

[2] Department of Geodesy and Geophysics, Cambridge University, Madingley Rise, Madingley Road, Cambridge CB 3 OEZ, England

Abstract. Two methods for tracing seismic rays between 2 given end points through three dimensional, continuously varying velocity structures are available. This paper describes and compares them for problems of practical interest and for analytical ray paths through an idealized velocity structure. One method involves "shooting" the ray from one point with a given starting direction and then modifying this starting direction until the ray emerges at the desired target, while the other method involves "bending" an initial path between the end points until it satisfies the principle of stationary time. For most of the models investigated, "bending" is computationally faster than "shooting" by a factor of 10 or more. The "bending" method can be modified to deal with discontinuities in the velocity model, and can also be adapted for use in conjunction with a table of distances as a function of ray parameter when the three dimensional anomaly influences only a small fraction of the total ray path. The geometrical spreading effect on the amplitude of the ray may be retrieved easily from the "bending" solution.

Key words: Seismic ray tracing – Geometrical optics.

Introduction

Recent studies of seismic wave propagation in structures such as descending lithospheric slabs and spreading ocean ridges have required the calculation of seismic ray paths through three dimensional velocity anomalies. From these studies we have gained an understanding of such phenomena as travel time anomalies in subduction zones (Jacob, 1970; Toksöz et al., 1971; Sorrels et al., 1971; Jacob, 1972; Sleep, 1973), shadow zones and amplitude anomalies (Julian, 1970; Toksöz et al., 1971; Davies and Julian, 1972) and distortion of apparent focal mechanisms (Toksöz et al., 1971; Solomon and Julian, 1974).

* To whom offprint requests should be sent

All of the seismic ray tracing for this work was accomplished by specifying the starting location and initial direction of the ray and treating it as an initial value problem. This method is efficient for calculating a family of rays through a structure, but there is no control over the point of emergence of any particular ray. In practice it is often necessary to determine a ray path between 2 specified end points, and in this paper 2 different approaches to the problem are considered. One approach is to make an estimate of the starting direction of the ray and then to solve the initial-value problem repeatedly, in a systematic attempt to refine the estimate of the starting direction. This method, which is commonly called *shooting*, has been used by Engdahl (1973) to calculate earthquake locations in the Aleutians Islands. The other method is to make an estimate of the ray path connecting the two end points and to modify this path, while keeping the end points fixed, until the ray becomes a stationary time path. This method, which we call *bending*, has been applied by Wesson (1971) to travel times near the San Andreas fault in central California. A different version of the bending method has been described by Chander (1975). The bending method described here differs slightly from both that of Wesson and that of Chander. Detailed mathematical discussions of numerical treatment of general two-point boundary value problems may be found in Keller (1968) and Roberts and Shipman (1972).

The Shooting Method

The shooting method involves integrating the initial value formulation of the problem, and employing a procedure for finding the starting direction which yields the desired ray.

The equations for the initial value problem may be cast in a particularly simple form if the ray path is specified parametrically in terms of position $\mathbf{r}(t)$, the parameter t being cumulative travel time, and a *slowness vector* $\boldsymbol{\sigma}(t)$ is defined as being tangent to the ray and having magnitude equal to the inverse of the local seismic wave speed, v. This definition gives us

$$\mathbf{r}' = v^2 \boldsymbol{\sigma}, \tag{1}$$

where the prime indicates differentiation with respect to t. The rate of change of slowness along the ray may be shown to be (Chernov, 1960)

$$\boldsymbol{\sigma}' = -\frac{\nabla v}{v}. \tag{2}$$

Equations (1) and (2) give a system of six first order differential equations which must be integrated numerically to find the ray path. However, since $|\boldsymbol{\sigma}| = \frac{1}{v}$, one equation is redundant, and may be eliminated. Appendix 1 gives computationally convenient forms of the equations in which the redundancy has been eliminated by expressing $\boldsymbol{\sigma}$ in terms of two angles giving its direction.

Several numerical methods are available for the purpose of integrating these ray equations; we have used the step-size extrapolation method of Bulirsch and Stoer (1966).

It remains to find the starting direction which causes the ray to pass through the desired end point. This involves finding solutions to two nonlinear simultaneous equations specified implicitly in terms of the differential Equations (1) and (2):

$$\begin{aligned} h(i_0, j_0) &= H, \\ g(i_0, j_0) &= G. \end{aligned} \tag{3}$$

Here h and g are the calculated coordinates (latitude and longitude, say) of the end of the ray with starting incidence angle i_0 and starting azimuth j_0. H and G are the coordinates of the end of the desired ray.

Two methods for solving Equations (3) suggest themselves: Newton's method and an extension of the method of False Position. Both methods have to be applied iteratively, since Equations (3) are generally nonlinear. In order to apply Newton's method it is necessary, at each stage of the iteration, to calculate the partial derivatives

$$\frac{\partial h}{\partial i_0}, \quad \frac{\partial h}{\partial j_0}, \quad \frac{\partial g}{\partial i_0} \quad \text{and} \quad \frac{\partial g}{\partial j_0}$$

and then to derive an improved estimate of i_0, j_0 by solving the system of linear equations

$$\begin{bmatrix} \frac{\partial h}{\partial i_0} & \frac{\partial h}{\partial j_0} \\ \frac{\partial g}{\partial i_0} & \frac{\partial g}{\partial j_0} \end{bmatrix} \begin{bmatrix} i_0^{(n+1)} - i_0^{(n)} \\ j_0^{(n+1)} - j_0^{(n)} \end{bmatrix} = \begin{bmatrix} H - h(i_0^{(n)}, j_0^{(n)}) \\ G - g(i_0^{(n)}, j_0^{(n)}) \end{bmatrix}, \tag{4}$$

where the superscripts indicate successive approximations to the root of Equations (3). The calculation of the partial derivatives is a laborious task. It involves solving two additional systems of ordinary differential equations (the "variational equations", see Keller, 1968) of the same order as the ray-path system (see Julian, 1970, for the explicit form of these equations).

The method of False Position involves the calculation of only the ray path at each iteration, but is expected to converge more slowly. At each stage of the iteration, an improved estimate of (i_0, j_0) is obtained by approximating the functions $h(i_0, j_0)$ and $g(i_0, j_0)$ by planes passing through the values calculated from three previous estimates. These planes take on the values H and G respectively, along two straight lines, whose intersection gives the desired improved estimate. The requisite equations may be written in the compact form (Acton, 1970):

$$\begin{vmatrix} i_0 - i_0^{(1)} & i_0 - i_0^{(2)} & i_0 - i_0^{(3)} \\ h^{(1)} - H & h^{(2)} - H & h^{(3)} - H \\ g^{(1)} - G & g^{(2)} - G & g^{(3)} - G \end{vmatrix} = 0$$

and similarly for j_0

$$\begin{vmatrix} j_0 - j_0^{(1)} & j_0 - j_0^{(2)} & j_0 - j_0^{(3)} \\ h^{(1)} - H & h^{(2)} - H & h^{(3)} - H \\ g^{(1)} - G & g^{(2)} - G & g^{(3)} - G \end{vmatrix} = 0$$

where the superscripts indicate the three previous estimates. This method has been adopted in this work.

The Bending Method

An alternative method for finding a seismic ray involves taking some initial estimate of the ray path and perturbing it, while keeping the ends fixed, until the true ray is found. This is essentially a variational approach. The differential equations for the ray are expressed in terms of changes in the ray path and linearized, and the resulting equations are solved by the finite-difference method. This involves the solution of a system of linear algebraic equations, where the matrix of coefficients is banded. As with the shooting method, the procedure must be applied iteratively, because the ray equations are nonlinear.

To derive the differential equations of the ray, we use Fermat's principle of stationarity of travel time with respect to small path variations. Consider a ray travelling from A to B through an inhomogeneous medium with wave speed v, and slowness $s = \frac{1}{v}$. The travel time, T_A^B, is given by:

$$T_A^B = \int_A^B \frac{dl}{v},$$

where dl is the arc length along the ray measured from some arbitrary point and the integral is taken along the true ray path. The ray path is described parametrically in Cartesian co-ordinates as:

$$x = x(q),$$
$$y = y(q),$$
$$z = z(q).$$

A choice for the parameter q will be made below. Let a dot denote differentiation with respect to q. For arc length l we have:

$$\frac{dl}{dq} = (\dot{x}^2 + \dot{y}^2 + \dot{z}^2)^{\frac{1}{2}} \equiv F \tag{5}$$

and the travel time becomes

$$T_A^B = \int_{q_A}^{q_B} sF \, dq. \tag{6}$$

The travel time may be made stationary by standard methods of the calculus of variations. The Euler equations are:

$$\frac{d}{dq}(sF)_{\dot{x}}=(sF)_x,$$

$$\frac{d}{dq}(sF)_{\dot{y}}=(sF)_y,$$

and

$$\frac{d}{dq}(sF)_{\dot{z}}=(sF)_z, \tag{7}$$

where $(sF)_x=\frac{\partial}{\partial x}(sF)$ and $(sF)_{\dot{x}}=\frac{\partial}{\partial \dot{x}}(sF)$, etc. These equations hold for any choice of the parameter q, which has not been specified. One of these equations is redundant. Multiply the first of Equations (7) by $\dot{x}$, the second by $\dot{y}$, the third by $\dot{z}$ and sum:

$$\frac{d}{dq}\{(sF)-[\dot{x}(sF)_{\dot{x}}+\dot{y}(sF)_{\dot{y}}+\dot{z}(sF)_{\dot{z}}]\}=0.$$

This is the familiar first integral form of the Euler equation for a variational problem when the integrand does not contain the independent variable explicity:

$$(sF)-\dot{x}(sF)_{\dot{x}}-\dot{y}(sF)_{\dot{y}}-\dot{z}(sF)_{\dot{z}}=\text{constant}.$$

Substituting for F reveals that this equation is *always* satisfied with the constant equal to zero. This proves that only two of Equations (7) are independent and we may delete the last one. The equation set must be completed by an expression defining q.

We are free to choose the parameter q that best suits our needs. We could take one of the spatial coordinates, $q=z$ say, and obtain only two equations to solve. However the rays would be defined by the functions $x(z)$ and $y(z)$ which can unfortunately be multiple-valued and can have infinite derivatives at turning points, even in very simple cases. Parameterizations of this sort have been used by Wesson (1971) and Chander (1975). q may be chosen to give a single-valued representation of the ray by making it a monotonic function of the arc length l. In this paper we make the simplest choice of:

$$q=\lambda\equiv l/L, \tag{8}$$

where L is the total length of the ray path from A to B. At the end points of the ray we have $\lambda=0$ (at A) and $\lambda=1$ (at B). From Equation (5) we see that $F=L$, a constant. Therefore

$$\frac{dF}{d\lambda}=0.$$

This choice for q has the advantage that it greatly simplifies the algebraic expressions for the first two differential Equations (7) (see Appendix 2). The full problem may be summarized:

$$\frac{d}{d\lambda}(sF)_{\dot{x}}=(sF)_x,$$

$$\frac{d}{d\lambda}(sF)_{\dot{y}}=(sF)_y,$$

$$\frac{dF}{d\lambda}=0, \tag{9}$$

with boundary conditions:

$$x(0)=x_A, \quad y(0)=y_A, \quad z(0)=z_A,$$

$$x(1)=x_B, \quad y(1)=y_B, \quad z(1)=z_B.$$

Equations (9) are written out in full in Appendix 2. They are nonlinear and are solved iteratively. Some initial path is chosen that passes through A and B, $\mathbf{x}^{(0)}(\lambda)=[x^{(0)}(\lambda), y^{(0)}(\lambda), z^{(0)}(\lambda)]$ and an improved estimate to the true ray is sought in the form:

$$\mathbf{x}^{(1)}(\lambda)=\mathbf{x}^{(0)}(\lambda)+\boldsymbol{\xi}^{(0)}(\lambda).$$

This is substituted into (9) and the resulting equations for $\boldsymbol{\xi}^{(0)}\equiv(\xi^{(0)}, \eta^{(0)}, \zeta^{(0)})$ are linearized and solved. The new estimate $\mathbf{x}^{(1)}$ will not be a true ray because of the linearization, but is used as the basis of a second improvement. Further iterations are carried out until the solution converges. Convergence is not guaranteed, but any converging solution must in the limit be a true ray path.

The first of Equations (9) may be written formally as:

$$\frac{d}{d\lambda}(sF)_{\dot{x}}-(sF)_x\equiv Q_1(\mathbf{x}, \dot{\mathbf{x}}, \ddot{\mathbf{x}})=0.$$

For the $(n+1)$-th iterate we have $\mathbf{x}^{(n+1)}=\mathbf{x}^{(n)}+\boldsymbol{\xi}^{(n)}$.
Substituting into (9) gives:

$$Q_1(\mathbf{x}^{(n)}, \dot{\mathbf{x}}^{(n)}, \ddot{\mathbf{x}}^{(n)})+\boldsymbol{\xi}^{(n)}\cdot\frac{\partial Q_1}{\partial \mathbf{x}}+\dot{\boldsymbol{\xi}}^{(n)}\cdot\frac{\partial Q_1}{\partial \dot{\mathbf{x}}}+\ddot{\boldsymbol{\xi}}^{(n)}\cdot\frac{\partial Q_1}{\partial \ddot{\mathbf{x}}}+O(\boldsymbol{\xi}^{(n)2}) \quad () \tag{10}$$

where each partial derivative is evaluated at $\mathbf{x}^{(n)}$. If $Q_2=0$ and $Q_3=0$ represent the last two equations of (9), the linearized equations for $\boldsymbol{\xi}^{(n)}$ may be written formally as:

$$\mathbf{B}^{(n)}\begin{bmatrix}\boldsymbol{\xi}^{(n)}(\lambda)\\ \dot{\boldsymbol{\xi}}^{(n)}(\lambda)\\ \ddot{\boldsymbol{\xi}}^{(n)}(\lambda)\end{bmatrix}=-\begin{bmatrix}Q_1[\mathbf{x}^{(n)}(\lambda)]\\ Q_2[\mathbf{x}^{(n)}(\lambda)]\\ Q_3[\mathbf{x}^{(n)}(\lambda)]\end{bmatrix}, \tag{11}$$

where the elements of the 3×9 matrix $\mathbf{B}^{(n)}$ are the partial derivatives of the Q's in Equation (10) and its analogs. The equations are written out in full in Appendix 2. The initial path, $\mathbf{x}^{(0)}$, is chosen to pass through A and B, so the boundary conditions on $\xi^{(n)}$ are:

$$\xi^{(n)}(0) = \xi^{(n)}(1) = 0. \tag{12}$$

The criterion used for convergence is that the root-mean-square path perturbation between successive iterations, given by

$$E^{(n)} = \left[\int_0^1 |\xi^{(n)}(\lambda)|^2 \, d\lambda \right]^{\frac{1}{2}},$$

be less than a given value comparable with the round-off error.

The second order differential Equations (11) with boundary conditions (12) are solved numerically. Second order finite difference techniques are used in preference to orthogonal function expansions (Galerkin methods) because rays often bend quite sharply and may not have the smooth properties desirable for, say, a Fourier representation. With $N+1$ finite difference points the differential equations are converted to a set of $3(N-1)$ algebraic equations in the unknowns

$\xi(\delta\lambda)$, $\xi(2\delta\lambda)$, ... where $\delta\lambda = 1/N$:

$$\mathbf{C}^{(n)} \begin{bmatrix} \xi(\delta\lambda) \\ \eta(\delta\lambda) \\ \zeta(\delta\lambda) \\ \xi(2\delta\lambda) \\ \vdots \\ \zeta([N-1]\,\delta\lambda) \end{bmatrix} = - \begin{bmatrix} Q_1(\delta\lambda) \\ Q_2(\delta\lambda) \\ Q_3(\delta\lambda) \\ Q_1(2\delta\lambda) \\ \vdots \\ Q_3([N-1]\,\delta\lambda) \end{bmatrix}. \tag{13}$$

The matrix $\mathbf{C}$ has the banded structure shown by the solid lines in Figure 1. The m-th row of blocks contains the coefficients of the three equations for the point $m\delta\lambda$. There are three submatrices on each line because, with second order finite differences, each equation relates variables at $m\delta\lambda$ to their values at $(m-1)\delta\lambda$ and $(m+1)\delta\lambda$ only. All other coefficients in the matrix are zero. The matrix $\mathbf{C}^{(n)}$ is stored as a rectangular matrix of size $11 \times 3(N-1)$, including all the elements within the solid brackets in Figure 1. Some elements of this matrix are still zero in the triangular pieces. The dashed parts of Figure 1 relate to generalized boundary conditions and internal surfaces of discontinuity, and are discussed later.

The algebraic Equations (13) are solved using standard techniques for banded matrices. The matrix is first factorized as:

$$\mathbf{C} = \mathbf{L}\mathbf{U}$$

where $\mathbf{L}$ has ones along the diagonal and nonzero elements below the diagonal, and is banded, and $\mathbf{U}$ contains nonzero elements on and above the diagonal, and is also banded. The equations then take the form

$$\mathbf{L}\mathbf{U}\mathbf{x} = \mathbf{b}$$

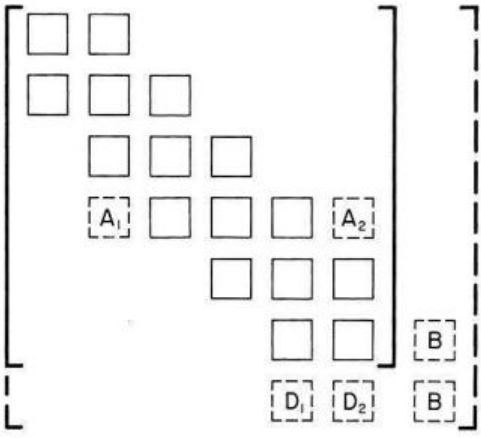

Fig. 1. The structure of the matrix **C** in Equation (13). Each block represents a 3×3 matrix. Elements of **C** outside these blocks are zero. The matrix for ordinary ray determination has only the solid blocks and is contained within the solid brackets. A discontinuity at $4\delta\lambda$ will entail the additional submatrices $\mathbf{A}_1$ and $\mathbf{A}_2$ because the discrete expression for Snell's law involves values at $2\delta\lambda$ and $6\delta\lambda$ as well as at $3\delta\lambda$, $4\delta\lambda$, and $5\delta\lambda$. The lower and upper triangles of $\mathbf{A}_1$ and $\mathbf{A}_2$ respectively must be reduced to zero by Gaussian elimination to retain the banded structure. If the generalized boundary condition (Eq. (16)) is used, the position values at $7\delta\lambda$ must be determined, which involves submatrices **B**. Derivatives at $7\delta\lambda$, if represented with second-order differences, entail values at $5\delta\lambda$ and $6\delta\lambda$, the coefficients of which are in submatrices $\mathbf{D}_1$ and $\mathbf{D}_2$. Again the lower left triangle of $\mathbf{D}_1$ must be made zero by Gaussian elimination to retain the banded structure

and are solved in two stages by Gaussian elimination. First we solve

$$\mathbf{L}\mathbf{y}=\mathbf{b}$$

for $\mathbf{y}$, and then solve

$$\mathbf{U}\mathbf{x}=\mathbf{y} \quad \text{for } \mathbf{x}.$$

The procedure is standard (Wilkinson, 1965). The factorization is the more time-consuming process and requires $O(N)$ operations compared with $O(N^3)$ for solving a full system. It is sometimes advisable, for the sake of stability, to rearrange matrix elements before solving. This can double the bandwidth of the matrix and increase computation time fourfold. Rearrangement of the matrix elements was not necessary for any of the calculations reported in this paper.

Numerical Test Cases

The first test example is taken from Barnes and Solomon (1973), who showed that the theory of complex variables may be used to derive the explicit functional forms of ray paths in cases when the logarithm of the wave speed is a two-dimensional harmonic function of position. The particular example chosen here is their case 4(c) in which the wave speed is given (in cartesian coordinates) by

$$v=[(x^2+y^2-1)^2+4y^2]^{\frac{1}{2}}. \tag{14}$$

The ray paths are hyperbolic cotangent spirals, expressed parametrically as

$$x=\frac{\sinh u}{\cosh u+\cos v}, \qquad y=\frac{\sin v}{\cosh u+\cos v}$$

where

$$u=C_1 \cos C_2+2t \sin C_2,$$

$$v=C_1 \sin C_2+2t \cos C_2.$$

C_1 and C_2 are constants and the parameter t is travel time. A contour plot of the wave speed in the model is given in Figure 2 and Figure 3 shows a typical ray path.

Two models of upper mantle heterogeneities have also been used as test cases. These are a model of the subduction zone in the central Aleutian Islands (Davies and Julian, 1972) and a model of a spreading oceanic ridge (Solomon and Julian, 1974). The Aleutian model is dominated by a high wave-speed lithospheric slab 80 km thick dipping northward into the mantle at an angle of 60 degrees and extending to a depth of about 230 km. The contrast in compressional wave speed between the slab and the surrounding mantle has a maximum value of 0.8 km/s (10%) at a depth of 100 km. The main feature of the oceanic ridge model is a region of extremely low wave speed lying beneath the ridge crest at depths between about 5 and 35 km. The contrast in compressional wave speed in this case has a maximum value of 1.0 km/s (12%) at a depth of 10 km. Figures showing these models and typical ray paths calculated for them may be found in the original references.

Accuracy

The absolute accuracy of the two methods can be assessed only for the analytical model for which the solution is known exactly. The accuracy of the ray path in the bending method should vary inversely with the cube of the mesh size because the finite-difference approximation is of second order and the truncation error is $O(\delta\lambda^3)$. In practice this is found to be the case, the actual exponent being slightly smaller than three, as would be expected because of errors other than truncation.

The accuracy of the shooting method is dependent upon the particular integration technique used to solve the initial-value problem, which in this paper is a step-size extrapolation method (Bulirsch and Stoer, 1966). The accuracy of such methods depends on the number of extrapolation steps used, and should be superior to that of ordinary finite-difference methods, for the same computational effort. In practice, this does not seem to be true. The accuracy of the shooting method is more than adequate, being limited by the machine word-length, but the computation time per iteration is greater than for the bending method.

Figure 4 compares the convergence of the bending and shooting methods for a typical example. All the test cases in this study exhibited very similar behavior.

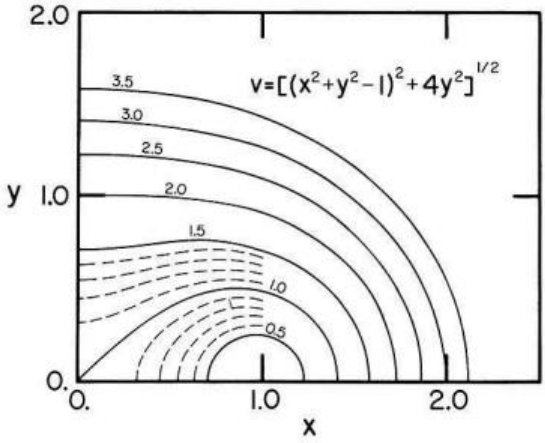

Fig. 2. Contour map of analytical wave speed model described in text. Only one quadrant is shown; the structure is symmetric with respect to reflection in the x and y axes

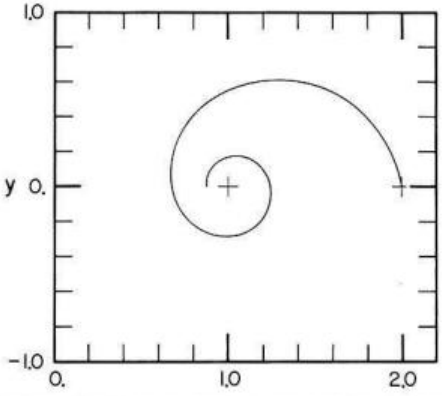

Fig. 3. A typical ray path corresponding to the model of Figure 2

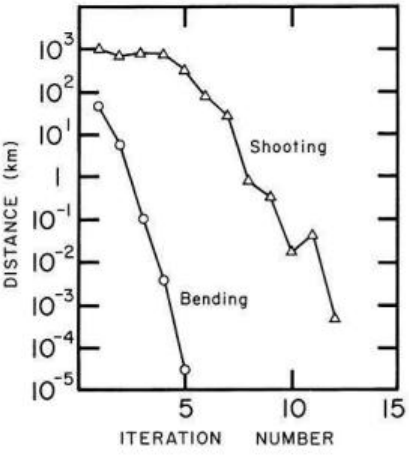

Fig. 4. Comparison of convergence speeds of the bending and shooting methods. For each iteration, the circles indicate the root-mean-square path perturbation for the bending method, while the triangles show the distance between the end of the ray and the desired end point for the shooting method

The shooting method required two to three times as many iterations, and was subjected to erratic behavior which depended critically upon the initial estimates of the starting direction. The use of Newton's method, Equation (4), would no doubt speed the convergence, but would greatly increase the time required for each step, and was not tried. The bending method, on the other hand, converged rapidly if a ray actually existed, and was quite insensitive to the particular starting estimate for the path used. This behavior, combined with its greater speed per iteration, made it greatly and clearly superior to the shooting method in these test examples.

Improvements to the Bending Method

Speeding up Convergence

Convergence for the bending method depends on the initial ray chosen. In all the numerical examples in this paper a straight line was drawn between the end points and used as a starting ray. In many realistic situations a better starting ray would be an arc of a circle or a ray traced through a spherically symmetric velocity structure. Also, a high degree of accuracy in intermediate iterations is not required and some economy is possible by performing early iterations with relatively few grid points and increasing the resolution only when the path has nearly converged to a ray.

The linear equation set (12) is solved by first factorizing the matrix into the form $\mathbf{L}\,\mathbf{U}$ (see Appendix 2) where $\mathbf{L}$ is lower triangular with unit diagonal elements and $\mathbf{U}$ is upper triangular, and then using Gaussian elimination. The factorization is the most time-consuming step, requiring $\frac{1}{2}m^2 n$ operations for a matrix of order n and band width m, compared with $\frac{1}{2}mn$ operations for the Gaussian elimination. Suppose that in Equation (13) instead of calculating and factorizing the matrix $\mathbf{C}^{(n)}$, we use the matrix from the previous iteration. The calculation can be speeded up considerably if several successive iterations are performed in this way before recomputing the correct matrix. If the iteration procedure does converge, it converges to a true ray (since the vanishing of the right-hand side of Equation (13) is the condition for a path to be a ray), even though the matrix is not updated at each step. However, convergence is expected to require more iterations.

Table 1 gives the results of this approach for a ray through the analytical velocity field given by Equation (14). The ray was found by both the standard bending method and the new method. The matrix was recomputed and factorized only after every 2, 5, and 10 iterations in each of three different cases. The most successful calculation was for factorizing every 5th iteration. The path converged after 14 iterations, but this represented only three factorizations of the matrix and required a time equivalent to about five full iterations.

Alternative Choices of the Independent Variable

In the formulation of the bending method the parameter q could be chosen arbitrarily. The calculations in this paper were performed entirely with $q=\lambda$. However, some improvement should be possible by choosing q so that the grid

Table 1

Number of iterations between each factorization	1	2	5	10
Total number of iterations required for convergence	7	13	14	Diverged after 13

points are more dense in parts of the ray path that are highly curved. One possibility is to make $\frac{dq}{dl}$ proportional to the radius of curvature, ρ, of the ray, which is given by

$$|\rho| = \frac{v}{|\nabla v \times \hat{\mathbf{n}}|}$$

where $\hat{\mathbf{n}}$ is the unit vector tangent to the ray:

$$\hat{\mathbf{n}} = \left(\frac{\dot{x}}{F}, \frac{\dot{y}}{F}, \frac{\dot{z}}{F}\right).$$

q is defined by

$$dq = |\rho| \, dl$$

and the third equation of (9) becomes, by Equation (5):

$$\frac{d}{dq}(\rho F) = 0.$$

The first two equations are now considerably more complicated than they were with $q = \lambda$. The resulting equations may be solved with the usual numerical techniques.

Generalization of the Boundary Conditions

So far, in discussing the bending method, the only boundary conditions at the ray ends which have been considered are those in which the locations of the end points are fixed:

$$\xi(0) = \xi(1) = 0. \tag{15}$$

It is straightforward to generalize this to a boundary condition consisting of a general inhomogeneous linear relation between the location of the end point and the ray direction there:

$$\mathfrak{F}\xi + \mathfrak{G}\dot{\xi} = \mathfrak{h} \tag{16}$$

where $\mathfrak{F}$ and $\mathfrak{G}$ are 3×3 matrices and $\mathfrak{h}$ is a column 3-vector. Particular forms of this generalization are very useful in problems of great practical importance.

The fixed boundary conditions for the ray tracing (Eq. (15)) are homogeneous and the equations governing the values of ξ at the end points are trivial. The terms in the equations which multiply $\xi(0)$ and $\xi(1)$ may therefore be omitted from the matrix $\mathbf{C}_n$ (Fig. 1). The generalized boundary condition of the form given by Equation (16) involves derivatives of ξ at $\lambda = 1$ say, which are represented by second order finite differences which involve the values of ξ at both $(1 - \delta\lambda)$ *and* $(1 - 2\delta\lambda)$. The latter terms introduce nonzero elements into $\mathbf{C}$ which are outside the bandwidth (Fig. 1). These elements may be removed by Gaussian elimination with one of the three preceding equations to restore the banded structure, so that matrix factorization can proceed as before.

As an example of the value of this boundary condition, consider the problem of tracing a ray through a structure that is mainly spherically symmetric, but contains some significant lateral variations in small regions, e.g. near the source or the receiver. Such problems are common in travel time studies of interesting tectonic areas (e.g. Engdahl et al., in press). The travel time through the deep, spherically symmetric region may be calculated from a predetermined table. The ray may be traced through the anomalous region, and the travel time through the deep region is expressed in terms of its ray parameter (or direction of emergence). As the iterative procedure for the bending method proceeds, the travel time through the symmetric region is re-computed and the total time converges on a stationary value.

Discontinuites in Wave Speed

An approach very similar to that used above to generalize the boundary conditions may also be used to treat cases in which the wave speed is discontinuous across a surface. An arbitrarily chosen mesh point is made to lie exactly on the surface. The wave speed derivatives do not exist here so the differential equations for the ray are replaced by Snell's law in the form of a jump condition. One more condition must be added to ensure that, after the perturbation, the mesh point still lies on the surface. The conditions may be linearized and cast in the form:

$$\mathfrak{F}\xi + \mathfrak{G}_2 \dot{\xi}_2 - \mathfrak{G}_1 \dot{\xi}_1 = \mathfrak{h} \tag{17}$$

where $\mathfrak{F}$, $\mathfrak{G}_1$, and $\mathfrak{G}_2$ are matrices and $\mathfrak{h}$ a vector, as before, and the subscripts 1 and 2 refer to the two sides of the surface. The jump condition will be satisfied in the limit as the ray converges, although, because of the linearization, it may not be satisfied at each step. Also, note that, since an arbitrarily selected mesh point has been put on the surface, the mesh spacing in the 2 regions will be different, though within each region it will be constant. When incorporating Equation (17) into the ray Equations (13), the derivatives of ξ are evaluated on each side of the discontinuity. Retaining second order accuracy involves the point on the boundary, say $\lambda = \Lambda$, and two additional points on each side of the discontinuity at Λ

$\pm\delta\lambda$ and $\Lambda\pm 2\delta\lambda$, as shown in Figure 1. This introduces nonzero elements in the matrix $\mathbf{C}$ which are outside of the bandwidth, and they must be made zero by Gaussian elimination before factorizing.

As an example, we give without proof the explicit form of $\mathfrak{F}$, $\mathfrak{G}$, and $\mathfrak{h}$ for the special case of a discontinuity across the surface $z=d$ in cartesian coordinates:

$$\mathfrak{F}=\begin{bmatrix} s_x^{(2)}\sin i^{(2)}-s_x^{(1)}\sin i^{(1)} & s_y^{(2)}\sin i^{(2)}-s_y^{(1)}\sin i^{(1)} & 0 \\ 0 & 0 & 0 \\ 0 & 0 & 1 \end{bmatrix},$$

$$\mathfrak{G}=\begin{bmatrix} \frac{s}{F}\cos i\cos j & \frac{s}{F}\cos i\sin j & -\frac{s}{F}\cos i\sin i \\ \frac{1}{\dot{x}}\tan i & -\frac{1}{\dot{x}} & 0 \\ 0 & 0 & 0 \end{bmatrix},$$

$$\mathfrak{h}=\begin{bmatrix} s^{(1)}\sin i^{(1)}-s^{(2)}\sin i^{(2)} \\ \tan i^{(2)}-\tan i^{(1)} \\ d-z \end{bmatrix}$$

where F is defined in Equation (5) and the quantities S, F, x, i, and j appearing in the expression for $\mathfrak{G}$ are to be given superscripts (1) or (2), as appropriate.

Calculation of Geometric Spreading

The calculation of the geometric spreading effect on the amplitudes of body waves turns out to be quite simple when the bending method is used.

Consider a known ray path between point 0, where there is a point source of intensity (power per unit solid angle) I, and point P, on the earth's surface. Let a tube of rays about this path that subtends a solid angle $d\Omega$ at 0 emerge at P over an area dA of the Earth's surface. Then if losses along the ray path are neglected, the power per unit area of wavefront at P, E say, is given by

$$I\,d\Omega = E\,dA\cos i_p,$$

where i_p is the angle between the ray and the downward-directed vertical at P. Let i_0 be the corresponding angle at 0 and j be the azimuth of the ray at 0. Then

$$d\Omega = \sin i_0\,di_0\,dj_0.$$

Also, if (r, θ_p, ϕ_p) are the spherical coordinates of P, then

$$dA = r^2\sin\theta_p\,d\theta_p\,d\phi_p,$$

so the geometric spreading ratio is

$$\frac{E}{I}=\frac{\sin i_0\,di_0\,dj_0}{r^2\sin\theta_p\cos i_p\,d\theta_p\,d\phi_p}=\frac{\sin i_0}{r^2\sin\theta_p\cos i_p}\,\frac{\partial(i_0, j_0}{\partial(\theta_p, \phi_p)},$$

where

$$\frac{\partial(i_0, j_0)}{\partial(\theta_p, \phi_p)} \equiv \begin{vmatrix} \frac{\partial i_0}{\partial \theta_p} & \frac{\partial j_0}{\partial \theta_p} \\ \frac{\partial i_0}{\partial \phi_p} & \frac{\partial j_0}{\partial \phi_p} \end{vmatrix}$$

is the Jacobian of the mapping from (i_0, j_0) to (θ_p, ϕ_p) defined by the ray paths.

The problem thus reduces to the evaluation of the partial derivatives $\frac{\partial i_0}{\partial \theta_p}$, $\frac{\partial j_0}{\partial \theta_p}$, $\frac{\partial i_0}{\partial \phi_p}$, $\frac{\partial j_0}{\partial \phi_p}$, which give the changes in the angles i_0 and j_0 corresponding to infinitesimal changes in θ_p and ϕ_p. Since the changes are infinitesimal, the differential equations for the changes in the ray path are linear. In fact, they are the same as the linearized equations used in computing the ray path, Equations (11), but with the right-hand side set to zero because, (r, θ, ϕ) is a true ray path. These equations must be solved twice, with boundary conditions $\xi = (0, d\theta_p, 0)$ and $\xi = (0, 0, d\phi_p)$. Since the equations are linear, these boundary conditions may be changed to $\xi = (0, 1, 0)$ and $\xi = (0, 0, 1)$ without loss of generality. Such inhomogeneous boundary conditions are easily cast in the form of Equation (16) and treated by the methods discussed above under "Generalization of the boundary conditions."

Summary

The comparison of methods in this paper shows that the bending method is the most efficient way to trace a ray between 2 given end points. With the modification for velocity discontinuities, the bending method can be applied to a wide range of problems of practical interest. It may be possible to improve "shooting" by using Newton's method, but this would involve solving additional equations at each step and it is unlikely to make the method faster than "bending."

Appendix I: Equations for the Initial Value Problem

Cartesian Coordinates. Eliseevnin (1965) has formulated the ray equations in a form that is convenient for solving the initial-value problem, namely:

$$\begin{aligned} x' &= v \cos\alpha, \\ y' &= v \cos\beta, \\ z' &= v \cos\gamma, \\ \alpha' &= v_x \sin\alpha - v_y \cot\alpha \cos\beta - v_z \cot\alpha \cos\gamma, \\ \beta' &= -v_x \cos\alpha \cot\beta + v_y \sin\beta - v_z \cot\beta \cos\gamma, \quad \text{and} \\ \gamma' &= -v_x \cos\alpha \cot\gamma - v_y \cos\beta \cot\gamma + v_z \sin\gamma. \end{aligned} \tag{A1.1}$$

The ray path is specified parametrically in terms of $x(t)$, $y(t)$ and $z(t)$, the cartesian coordinates as functions of the accumulated travel time t. $\alpha(t)$, $\beta(t)$, and $\gamma(t)$ are the direction angles of the tangent to the ray. The seismic velocity, v, and its spatial derivatives v_x, v_y, and v_z are specified functions of position. Prime represents differentiation with respect to time.

Since $\cos^2\alpha+\cos^2\beta+\cos^2\gamma=1$, the Equations (A1.1) are not independent, and one may be eliminated. A convenient way to do this is to transform to the angle i which the ray tangent makes with the z axis and the angle j which the vertical plane tangent to the ray makes with the x axis. If the $+z$ axis is directed vertically downwards, these angles may be identified as the conventional seismological "angle of incidence" and the azimuth of the ray, and are related to α, β, and γ by

$$\begin{aligned} \gamma &\equiv i, \\ \cos\alpha &= \sin i \cos j, \\ \cos\beta &= \sin i \sin j. \end{aligned} \tag{A1.2}$$

The system of Equations (A1.1) becomes

$$\begin{aligned} x' &= v \sin i \cos j, \\ y' &= v \sin i \sin j, \\ z' &= v \cos i, \\ i' &= -\cos i [v_x \cos j + v_y \sin j] + v_z \sin i, \end{aligned}$$

and

$$j' = \frac{1}{\sin i}[v_x \sin j - v_y \cos j]. \tag{A1.3}$$

Spherical Coordinates. Equations analogous to (A1.3) in which the ray path is defined by its spherical coordinates as functions of time, $r(t)$, $\theta(t)$, and $\phi(t)$, have been derived by Julian (1970).

$$\begin{aligned} \gamma' &= -v \cos i, \\ \theta' &= -\frac{v}{\gamma} \sin i \cos j, \\ \phi' &= \frac{v}{\gamma \sin\theta} \sin i \sin j, \\ i' &= \left(v_r - \frac{v}{r}\right) \sin i - \cos i \left(\frac{v_\theta}{r} \cos j - \frac{v_\phi}{r \sin\theta} \sin j\right), \end{aligned}$$

and

$$j' = \frac{1}{\sin i}\left(\frac{v_\theta}{r} \sin j + \frac{v_\theta}{r \sin\theta} \cos j\right) - \frac{v}{r} \sin i \sin j \cot\theta. \tag{A1.4}$$

As before, $i(t)$ is the angle between the ray tangent and the vertical ($i=0$ indicating a downward directed ray). $j(t)$ is the angle which the vertical plane

tangent to the ray makes with the meridional plane. $j=0$ indicates a ray directed in the $-\theta$ direction, and increasing j indicates clockwise rotation, when viewed from above, in accordance with the conventional definition of azimuth.

Appendix 2: "Bending" Equations for the Boundary Value Problem

Equations (9) may be written out in full in terms of the parametric ray representation $x(\lambda)$, $y(\lambda)$, and $z(\lambda)$ as:

$$Q_1 = -s_x(\dot{y}^2+\dot{z}^2)+s_y\dot{x}\dot{y}+s_z\dot{x}\dot{z}+s\ddot{x}=0,$$
$$Q_2 = -s_y(\dot{x}^2+\dot{z}^2)+s_x\dot{x}\dot{y}+s_z\dot{y}\dot{z}+s\ddot{y}=0,$$

and

$$Q_3 = \dot{x}\ddot{x}+\dot{y}\ddot{y}+\dot{z}\ddot{z}=0. \tag{A2.1}$$

These equations have been simplified using the third equation, $\frac{dF}{d\lambda}=0$. To derive the iteration procedure, substitute $\mathbf{x}^{(n+1)}=\mathbf{x}^{(n)}+\boldsymbol{\xi}^{(n)}$ into these equations and linearize in $\boldsymbol{\xi}^{(n)}$. Dropping supercripts n, we have

$$\begin{aligned}
&s\ddot{\xi}+(s_z\dot{z}+s_y\dot{y})\dot{\xi}+[s_{xy}\dot{x}\dot{y}+s_{xz}\dot{x}\dot{z}+s_x\ddot{x}-s_{xx}(\dot{y}^2+\dot{z}^2)]\,\xi\\
&\quad+(s_y\dot{x}-2s_x\dot{y})\dot{\eta}+[s_{yy}\dot{x}\dot{y}+s_{yz}\dot{x}\dot{z}+s_y\ddot{x}-s_{xy}(\dot{y}^2+\dot{z}^2)]\,\eta\\
&\quad+(s_z\dot{x}-2s_x\dot{z})\dot{\zeta}+[s_{yz}\dot{x}\dot{y}+s_{zz}\dot{x}\dot{z}+s_z\ddot{x}-s_{xz}(\dot{y}^2+\dot{z}^2)]\,\zeta=-Q_1,
\end{aligned}$$

$$\begin{aligned}
&(s_x\dot{y}-2s_y\dot{x})\dot{\xi}+[s_{xx}\dot{x}\dot{y}+s_{xz}\dot{y}\dot{z}+s_x\ddot{y}-s_{xy}(\dot{x}^2+\dot{z}^2)]\,\xi\\
&\quad+s\ddot{\eta}+(s_x\dot{x}+s_z\dot{z})\dot{\eta}+[s_{xy}\dot{x}\dot{y}+s_{yz}\dot{y}\dot{z}+s_y\ddot{y}-s_{yy}(\dot{x}^2+\dot{z}^2)]\,\eta\\
&\quad+(s_z\dot{y}-2s_y\dot{z})\dot{\zeta}+[s_{xz}\dot{x}\dot{y}+s_{zz}\dot{y}\dot{z}+s_z\ddot{y}-s_{yz}(\dot{x}^2+\dot{z}^2)]\,\zeta=-Q_2,
\end{aligned}$$

and

$$\dot{x}\ddot{\xi}+\ddot{x}\dot{\xi}+\dot{y}\ddot{\eta}+\ddot{y}\dot{\eta}+\dot{z}\ddot{\zeta}+\ddot{z}\dot{\zeta}=-Q_3. \tag{A2.2}$$

The velocity model will generally be specified in spherical coordinates. It is possible to convert to cartesian coordinates and solve for the ray the equation set (A2.2), or alternatively, the problem can be cast entirely in spherical coordinates. In the latter case, complications arise when the ray passes through the center or axis of the coordinate system. For the spherical coordinate system, Equations (A2.1) become:

$$Q_1 = s\ddot{r}-(r^2s_r+rs)(\dot{\theta}^2+\sin^2\theta\dot{\phi}^2)+s_\theta\dot{r}\dot{\theta}+s_\phi\dot{r}\dot{\phi}=0,$$
$$Q_2 = p\ddot{\theta}-s_\theta\dot{r}^2-p_\theta\sin^2\theta\dot{\phi}^2-p\sin\theta\cos\theta\dot{\phi}^2+p_r\dot{r}\dot{\theta}+p_\phi\dot{\theta}\dot{\phi}=0,$$

and

$$Q_3 = \dot{r}\ddot{r}+r\dot{r}\dot{\theta}^2+r^2\dot{\theta}\ddot{\theta}+r\dot{r}\sin^2\theta\dot{\phi}^2+r^2\sin\theta\cos\theta\dot{\theta}\dot{\phi}^2+r^2\sin^2\theta\dot{\phi}\ddot{\phi}=0, \tag{A2.3}$$

where $p=r^2s$. The iteration procedure is derived by substituting

$$r^{(n+1)}=r^{(n)}+\xi^{(n)},\quad \theta^{(n+1)}=\theta^{(n)}+\eta^{(n)}\quad\text{and}\quad \phi^{(n+1)}=\phi^{(n)}+\zeta^{(n)},$$

and linearizing:

$$\ddot{\xi}s+\dot{\xi}[s_\theta\dot{\theta}+s_\phi\dot{\phi}]$$
$$+\xi[s_r\ddot{r}-(3rs_r+r^2s_{rr}+s)(\dot{\theta}^2+\sin^2\theta\dot{\phi}^2)+s_{r\theta}\dot{r}\dot{\theta}+s_{r\phi}\dot{r}\dot{\phi}]$$
$$+\dot{\eta}[-2(r^2s_r+rs)\dot{\theta}+s_\theta\dot{r}]+\eta[-2(r^2sr+rs)\sin\theta\cos\theta\dot{\phi}^2$$
$$+s_\theta\ddot{r}+s_{\theta\theta}\dot{r}\dot{\theta}+s_{\theta\phi}\dot{r}\dot{\phi}-(r^2s_{r\theta}+rs_\theta)(\dot{\theta}^2+\sin^2\theta\dot{\phi}^2)]$$
$$+\dot{\zeta}[-2(r^2s_r+rs)\sin^2\theta\dot{\phi}+s_\phi\dot{r}]$$
$$+\zeta[s_\phi\ddot{r}-(r^2s_{r\phi}+rs_\phi)(\dot{\theta}^2+\sin^2\theta\dot{\phi}^2)+s_{\theta\phi}\dot{r}\dot{\theta}+s_{\phi\phi}\dot{r}\dot{\phi}]=-Q_1, \qquad \text{(A2.4)}$$

$$\ddot{\xi}[-2s_\theta\dot{r}+p_r\dot{\theta}]+\xi[p_r\ddot{\theta}-s_{r\theta}\dot{r}^2-p_{r\theta}\sin^2\theta\dot{\phi}^2-p_r\sin\theta\cos\theta\dot{\phi}^2$$
$$+p_{rr}\dot{r}\dot{\theta}+p_{r\phi}\dot{\theta}\dot{\phi}]+\ddot{\eta}p+\dot{\eta}[p_r\dot{r}+p_\phi\dot{\phi}]$$
$$+\eta[p_\theta\ddot{\theta}-s_{\theta\theta}\dot{r}^2-p_{\theta\theta}\sin^2\theta\dot{\phi}^2-3p_\theta\sin\theta\cos\theta\dot{\phi}^2$$
$$-p\cos^2\theta\dot{\phi}^2+p_{r\theta}\dot{r}\dot{\theta}+p_{\theta\phi}\dot{\theta}\dot{\phi}]$$
$$+\dot{\zeta}[-2p_\theta\sin^2\theta\dot{\phi}-2p\sin\theta\cos\theta\dot{\phi}+p_\phi\dot{\theta}]$$
$$+\zeta[p_\phi\ddot{\theta}-s_{\theta\phi}\dot{r}^2-p_{\theta\phi}\sin^2\theta\dot{\phi}^2-p_\phi\sin\theta\cos\theta\dot{\phi}^2$$
$$+p_{r\phi}\dot{r}\dot{\theta}+p_{\phi\phi}\dot{\theta}\dot{\phi}]=-Q_2.$$

and

$$\ddot{\xi}\dot{r}+\dot{\xi}[\ddot{r}+r(\dot{\theta}^2+\sin^2\theta\dot{\phi}^2)]$$
$$+\xi[\dot{r}\dot{\theta}^2+2r\dot{\theta}\ddot{\theta}+\dot{r}\sin^2\theta\dot{\phi}^2+2r(\sin\theta\cos\theta\dot{\theta}\dot{\phi}^2+\sin^2\theta\dot{\phi}\ddot{\phi})]+\ddot{\eta}r^2\dot{\theta}$$
$$+\dot{\eta}[2r\dot{r}\dot{\theta}+r^2\ddot{\theta}+r^2\sin\theta\cos\theta\dot{\phi}^2]$$
$$+\eta[2r\dot{r}\sin\theta\cos\theta\dot{\phi}^2+r^2\cos2\theta\dot{\theta}\dot{\phi}^2+2r^2\sin\theta\cos\theta\dot{\phi}\ddot{\phi}]$$
$$+\ddot{\zeta}r^2\sin^2\theta\dot{\phi}+\dot{\zeta}[2r\dot{r}\sin^2\theta\dot{\phi}+2r^2\sin\theta\cos\theta\dot{\theta}\dot{\phi}+r^2\sin^2\theta\ddot{\phi}]=-Q_3.$$

References

Acton, F.: Numerical methods that work. New York: Harper and Row 1970

Barnes, A., Solomon, L.P.: Some curious analytical ray paths for some interesting velocity profiles in geometrical acoustics. J. Acoustical Soc. Am. **53**, 147–155, 1973

Bulirsch, R., Stoer, J.: Numerical treatment of ordinary differential equations by extrapolation methods. Numer. Math. **8**, 1–13, 1966

Chander, R.: On tracing seismic rays with specified end points. J. Geophys. **41**, 173–177, 1975

Chernov, L.A.: Wave propagation in a random medium. New York: Dover 1960

Davies, D., Julian, B.R.: A study of short period *P*-wave signals from Longshot. Geophys. J. **29**, 185–202, 1972

Eliseevnin, V.A.: Analysis of waves propagating in an inhomogeneous medium. Soviet Physics-Acoustics **10**, 242–245, 1965

Engdahl, E.R.: Relocation of intermediate depth earthquakes in the central Aleutians by seismic ray tracing. Nature Phys. Sci. **245**, 23–25, 1973

Engdahl, E.R., Sleep, N.H., Lin, M.T.: Plate effects in North Pacific subduction zones. Tectonophysics **37**, 95–116, 1977

Jacob, K.H.: Three-dimensional seismic ray tracing in a laterally heterogeneous spherical earth. J. Geophys. Res. **75**, 6685–6689, 1970

Jacob, K.H.: Global tectonic implications of anomalous seismic *P* travel times from the nuclear explosion Longshot. J. Geophys. Res. **77**, 2556–2573, 1972

Julian, B.R.: Ray tracing in arbitrarily heterogeneous media. Tech. Note 1970–45, Lincoln Laboratory. Mass. Inst. of Tech., Lexington, Mass., 1970

Keller, H.B.: Numerical methods for two-point boundary-value problems. Waltham, Mass.: Blaisdell 1968

Roberts, S.M., Shipman, J.S.: Two-point boundary value problems: Shooting methods. New York: Elsevier 1972

Sleep, N.H.: Teleseismic *P*-wave transmission through slabs. Bull. Seism. Soc. Am. **63**, 1349–1373, 1973

Solomon, S.C., Julian, B.R.: Seismic constraints on ocean-ridge mantle structure: Anomalous fault-plane solutions from first motions. Geophys. J. **38**, 265–285, 1974

Sorrels, G.G., Crowley, J.B., Veith, K.F.: Methods for computing ray paths in complex geological structures. Bull. Seism. Soc. Am. **61**, 27–53, 1971

Toksöz, M., Nafi, J., Minear, W., Julian, B.R.: Temperature field and geophysical effects of a downgoing slab. J. Geophys. Res. **76**, 1113–1138, 1971

Wesson, R.L.: Travel-time inversion for laterally inhomogeneous crustal velocity models. Bull. Seism. Soc. Amer. **61**, 729–746, 1971

Wilkinson, J.H.: The algebraic eigenvalue problem. Oxford: Clarendon Press 1965

Received October 13, 1976